Economic Geology, v. 117, no. 1, pp. 237–252

DIRECT Re-Os DATING OF MANGANESE CARBONATE ORES AND IMPLICATIONS FOR THE FORMATION OF THE ORTOKARNASH MANGANESE DEPOSIT, NORTHWEST CHINA

Wen-Jun Li,[1,2,3,*] Zi-Dong Peng,[1,2,*] Zhi-Guo Dong,[1,2,3] Bang-Lu Zhang,[4,5,6] Bing-Yu Gao,[1,2,3] Lian-Chang Zhang,[1,2,3,†] Ming-Tian Zhu,[1,2] Leslie J. Robbins,[7] and Kurt O. Konhauser[8]

[1]*Key Laboratory of Mineral Resources, Institute of Geology and Geophysics, Chinese Academy of Sciences, Beijing 100029, China*

[2]*Innovation Academy for Earth Science, Chinese Academy of Sciences, Beijing 100029, China*

[3]*University of Chinese Academy of Sciences, Beijing 100049, China*

[4]*Development and Research Center, China Geological Survey, Beijing 100037, China*

[5]*China University of Geosciences, Beijing 100083, China*

[6]*Mineral Exploration Technical Guidance Center, Ministry of Natural Resources of the People's Republic of China, Beijing 100083, China*

[7]*Department of Geology, University of Regina, Regina, Saskatchewan S4S 0A2, Canada*

[8]*Department of Earth and Atmospheric Sciences, University of Alberta, Edmonton, Alberta T6G 2E3, Canada*

Abstract

Sedimentary manganese carbonate deposits, the major economic source of Mn globally, are the product of complex interactions that occur in the marine environment, including both biological Mn(II) oxidation and Mn(IV) reduction. Precise and accurate age constraints for Mn carbonate deposits have been difficult to obtain, hindering the understanding of possible correlations between Mn metallogenic and paleoenvironmental processes at regional to global scale. The involvement of organic matter during Mn carbonate mineralization, however, allows for the Re-Os system, an ideal geochronological tool for determining the depositional or alteration ages of organic-rich rocks, to be applied. Here we present the first Re-Os systematics of Mn carbonate ores from the giant Ortokarnash Mn deposit in the West Kunlun orogenic belt, Xinjiang, China. The use of the Re-Os geochronometer, along with petrographic, whole-rock total organic carbon, and major element analyses, allows for the depositional age and mineralizing processes to be directly constrained. The Mn carbonate ores with relatively homogeneous initial $^{187}Os/^{188}Os$ values yield a robust mineralization age of 320.3 ± 6.6 Ma (Model 1; Isoplot regression) or 321.8 ± 14.5 Ma (Monte Carlo simulation). This age correlates well with U-Pb ages of the youngest detrital zircon group from the footwall volcanic breccia-bearing limestone and a newly obtained Re-Os age from the hanging-wall marlstones. Enrichment of hydrogenous Re and Os in the Ortokarnash Mn carbonate ores is likely related to the variable redox environments during Mn carbonate mineralization, where Re tends to be preserved in the organic matter that persists following the diagenetic reduction of the Mn(IV) oxyhydroxides in suboxic or anoxic sediment pore water. Conversely, Os was likely absorbed by Mn(IV) oxyhydroxides in oxic seawater during Mn(II) oxidation. Elevated $Os_{initial(i)}$ for the Mn carbonate ores relative to that of the coeval global seawater value suggests that an increased riverine flux may have been a contributing factor leading to Mn mineralization.

Introduction

Sedimentary manganese carbonate deposits are Earth's most significant source of Mn (Maynard, 2010). The importance of Mn carbonate deposits is exemplified by numerous studies that provide key insights into processes such as paleoclimatic fluctuations, volcanic and hydrothermal activity, as well as redox changes that have contributed to shaping the Earth's surface (Calvert and Pedersen, 1996; Liu et al., 2006; Maynard, 2014; Johnson et al., 2016). Understanding the mineralization age of Mn carbonate deposits is a prerequisite to reconstructing the relationships between mineralization and regional or global geologic process. However, age control in most sedimentary Mn deposits is often hampered by the lack of reliable biostratigraphic constraints and/or the absence of tuff horizons suitable for zircon U-Pb dating, making the direct dating of these deposits a challenge.

†Corresponding author: e-mail, lczhang@mail.iggcas.ac.cn
*Wen-Jun Li and Zi-Dong Peng contributed equally to this paper.

Rhenium-osmium geochronology has been demonstrated to be a powerful tool for constraining the depositional age of sedimentary rocks, such as marine mudrocks (Creaser et al., 2002; Selby et al., 2009), organic-rich limestones (Rooney et al., 2012; Kendall et al., 2013), lacustrine shales (Cumming et al., 2012; Pietras et al., 2020), and marine-influenced coals (Tripathy et al., 2015; Rotich et al., 2021). Simultaneously, the Re-Os system is also able to provide critical information on the Os isotope composition of coeval seawater, and how it responds to either localized or global environmental impacts, including the Great Oxidation Event (Hannah et al., 2004; Kendall et al., 2013), glacial and interglacial cycles (Finlay et al., 2010; Rooney et al., 2020), and biotic crises (Selby et al., 2009; Xu et al., 2014). Normally, organic-rich sediments, which are deposited and underlie suboxic or anoxic bottom waters, represent ideal rocks for Re-Os dating because high concentrations of Re and Os, as well as variable isotopic compositions controlled by organic matter and/or sulfides, are common (Hannah et al., 2006; Tripathy et al., 2014). In oxy-

ISSN 0361-0128; doi:10.5382/econgeo.4865; 16 p.

Submitted: December 30, 2020 / Accepted: April 2, 2021

genated marine environments, elevated Os concentrations are typical in ferromanganese crusts and Mn nodules, and thus their Os isotope compositions can be used either as paleomarine environmental tracers or to develop model ages (Burton et al., 1999; Tokumaru et al., 2015; Conrad et al., 2017; Josso et al., 2019).

Although distinct from the deposits mentioned above, sedimentary Mn carbonate deposits are widely accepted as being a diagenetic product of Mn(IV) oxyhydroxides reduction (Calvert and Pedersen, 1996; Johnson et al., 2016). This means that Mn carbonate deposits commonly form via a two-stage process: (1) Mn(II) oxidation in the water column, followed by (2) Mn(IV) reduction coupled to organic matter oxidation in anoxic pore waters of the sediment pile (Tebo et al., 2004; Dick et al., 2009; Hansel et al., 2012). Given that organic matter is essential for the diagenetic formation of massive Mn carbonate ores, it should be possible to apply Re-Os geochronology to Mn carbonate ores; however, this possibility has yet to be thoroughly evaluated. Furthermore, seawater initial $^{187}Os/^{188}Os$ (Os_i) values reflect the balance between radiogenic continental runoff and aeolian dust, mantle-derived unradiogenic hydrothermal solutions or cosmic dust (Peucker-Ehrenbrink and Ravizza, 2000). These isotopically distinct inputs, in combination with the short marine residence time (10^3–10^4 yr) of Os (Peucker-Ehrenbrink and Ravizza, 2020 and references therein), makes it a favorable tracer to probe rapid variations in response to a variety of environmental fluctuations (Ravizza and Peucker-Ehrenbrink, 2003; Finlay et al., 2010). Taking this into account, the Os_i values of Mn carbonate ores also have the potential to provide further insights into the processes driving Mn mineralization.

In this study, we present whole-rock Re-Os isotopes, major element chemistry, and total organic carbon (TOC) contents for the Mn carbonate ores of the Ortokarnash Mn deposit and its associated host rocks in the Xinjiang province, China. We evaluate the potential of Re-Os systematics to yield geochronological information for Mn carbonate ores. Further, insights into the mineralization processes are gained by evaluating Os_i values relative to select elements (Mn, Al, Re, and Os) in both the Mn carbonate ores and associated rocks. Overall, this study demonstrates the utility in using Re-Os systematics to constrain the mineralization age and ore-forming processes of sedimentary Mn carbonate deposits.

Geologic Background

The Ortokarnash Mn deposit, an important part of the Malkansu Mn metallogenic belt, is located in the northern section of West Kunlun orogenic zone in western China (Fig. 1A). The orogen is bounded to the north by the Tarim basin and to the south by the Tibetan plateau. From north to south, it can be divided into three main units, the North Kunlun, South Kunlun, and Tianshuihai terranes (Fig. 1B) (Yin and Harrison, 2000; Pan and Fang, 2010). The Malkansu Mn metallogenic belt is 60 km in length and 2 km in width, and is situated in the North Kunlun terrane (Gao et al., 2018; Zhang et al., 2018). This metallogenic belt encompasses the active Ortokarnash Mn deposit and two prospects (Muhu and Malkantu), as well as several smaller occurrences of Mn mineralization.

The Mn deposits occur mainly as part of a Carboniferous to Permian volcano-sedimentary back-arc basin sequence in the North Kunlun terrane (Gao et al., 2018). These stratabound Mn-rich lithologies and their associated host rocks can be grouped into three formations with unconformable or fault contacts. The lowermost Wuluate Formation consists of early Carboniferous basalt flows and associated pyroclastic rocks, which mainly occupy the eastern portion of the Malkansu Mn metallogenic belt. The overlying Upper Carboniferous Kalaatehe Formation is composed of (volcanic) breccia limestone, sandy limestone, and marlstone (Zhang et al., 2020). The uppermost Permian Maerkanque-Kusaishan Formation unconformably overlies the Carboniferous Kalaatehe Formation, which consists of a gray-purple conglomerate, andesitic tuff, and minor andesite, and is capped by a thick-bedded crystalline limestone (Zhang et al., 2018, 2020).

The Ortokarnash Mn deposit is located at the westernmost end of the Malkansu Mn metallogenic belt. The stratabound deposit is approximately 5 km long and less than 2 km wide (Fig. 1C). Exposed strata in this area include Mn-bearing sedimentary rocks of the upper Carboniferous Kalaatehe Formation, volcano-sedimentary rocks of the Permian Maerkanque-Kusaishan Formation, and terrigenous sedimentary rocks of the Cretaceous Kukebai Formation. In addition, there is a large Quaternary cover in the south-central mine area. An approximately E-W–trending fault (F_1) runs through the mine and NE-trending secondary faults (F_2) also developed to produce a minor offset between the orebody and the host rocks (Fig. 1C). The ore-bearing Kalaatehe Formation, for which the deposition corresponds to a marine transgression, can be further divided into three members (Fig. 2). In ascending order these are as follows: (1) Member 1, which consists mainly of volcanic breccia-bearing limestone; (2) Member 2, composed of sandy limestone with occurrences of fossils such as corals and crinoid debris, and (3) Member 3, which includes marlstone, limestone, and two layers of Mn carbonate ores (Gao et al., 2018; Zhang et al., 2018). The fossil occurrences in Member 2 provide some biostratigraphic evidence of Late Carboniferous deposition (Zhang et al., 2018). Two intervals of Mn mineralization are interbedded with organic-rich marlstone: the lower, main layer is stratigraphically continuous with an average thickness of 6 m and an average Mn content of more than 37% by weight. In contrast, the upper layer is discontinuous and occurs as an outcrop with a limited thickness of 1 m.

Sample Preparation and Analytical Methods

Sample preparation

A suite of 22 samples, including seven marlstones from the footwall, nine Mn carbonate ore samples, and six marlstone samples from the hanging wall, were collected from a ~20-m-thick, continuous Mn-bearing sequence in Member 3 of Kalaatehe Formation. This is the major Mn layer at the Ortokarnash mine. The collected marlstones can be further divided into organic-rich and organic-poor groups. The former includes nine samples with TOC >1%, six from the hanging wall and three from the footwall. The organic-poor group, in contrast, is composed of four samples from the footwall characterized by a TOC <1%.

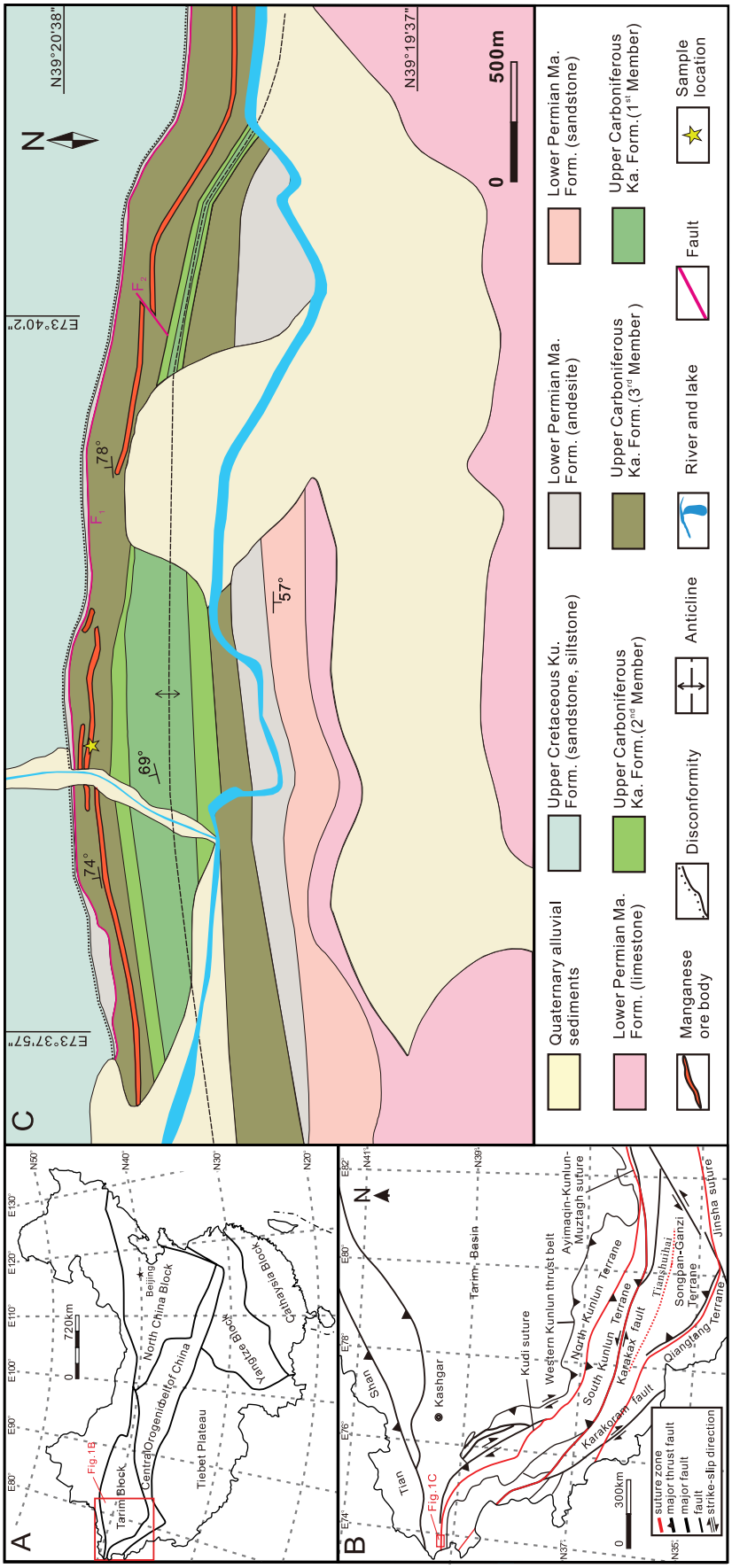

Fig. 1. (A) Location map of the West Kunlun orogenic zone in China (modified from Fan and Yang, 1999); (B) Simplified tectonic units of the West Kunlun orogenic zone (modified from Zhang et al., 2020); (C) Geologic map of the Ortokarnash manganese deposit showing distributions of the orebodies and associated rocks (modified from Zhang et al., 2020). Abbreviations: Form. = Formation, Ka.= Kalaatehe, Ku. = Kukebai, Ma. = Maerkanque-Kusaishan.

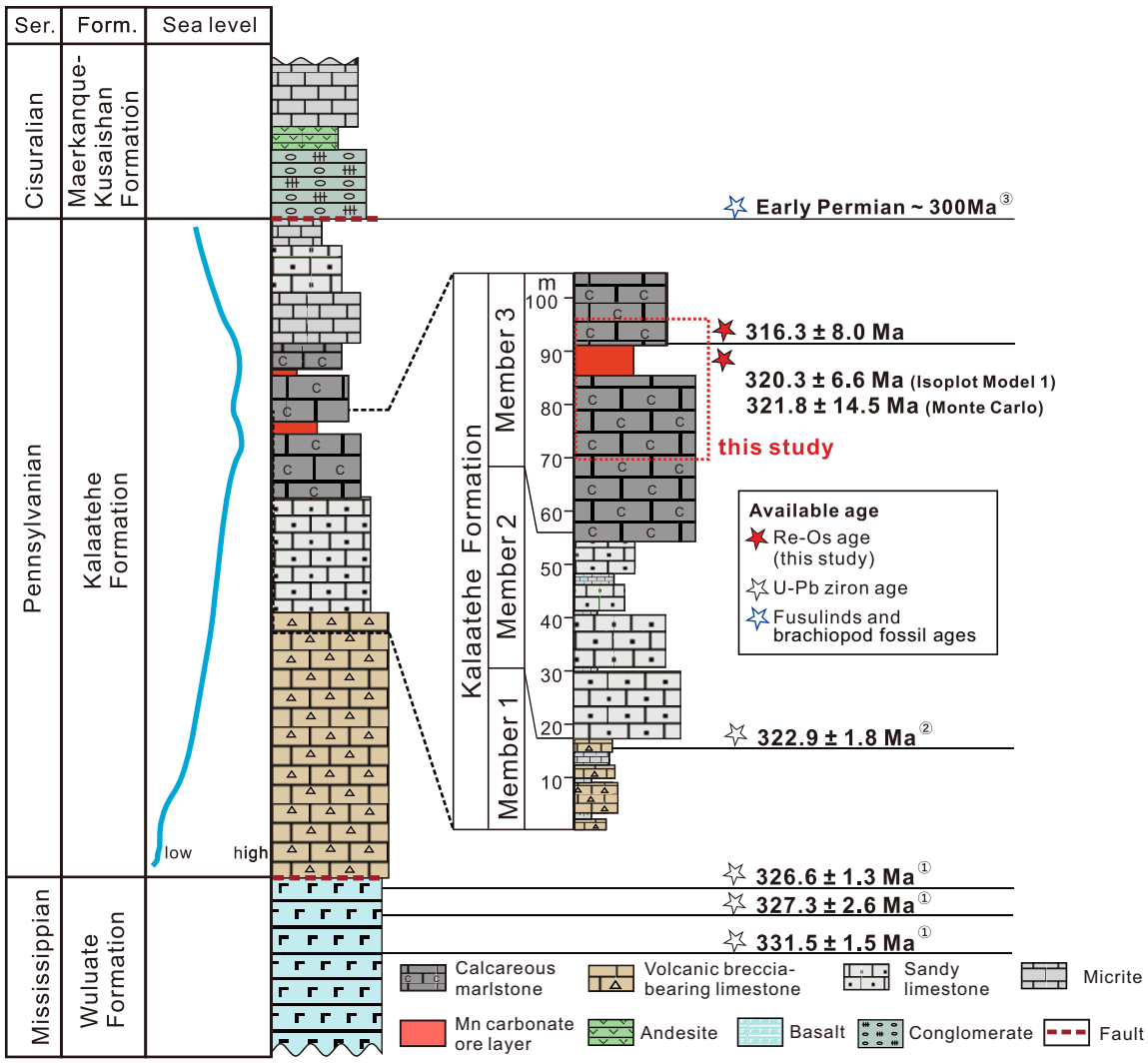

Fig. 2. Stratigraphic section of Carboniferous-early Permian sedimentary rocks of Malkansu, highlighting the Kalaatehe Formation composed of three members and the interval of manganese mineralization. Isotope data of samples indicated with red stars are presented in Table 2 and Figure 5. Previous published age constraints are from U-Pb zircon ages: ① Gao et al., 2018, ② Zhang, 2020 and biostratigraphic age, ③ Gao, 2015.

Three representative polished thin sections (namely, organic-rich and/or -poor marlstone and Mn carbonate ore samples) were prepared and examined using transmitted and reflected light microscopy in order to determine the mineralogy and textural relationships of the Mn ore and the associated host rocks. A high-resolution field emission scanning electron microscope (FE-SEM; FEI Nova NanoSEM 450) operating at 15 kV and spot size of 5.5 was used to perform visualization and imaging of the microstructure of Mn carbonate ore samples. To reveal the elemental distribution of samples, energy-dispersive X-ray spectroscopy (EDS) data were collected with Oxford X-Max^{N}80mm^2 EDS detectors attached to FEI SEM at 15 kV. The SEM analyses were conducted at the Institute of Geology and Geophysics, Chinese Academy of Sciences (IGGCAS) in Beijing.

Geochemical methods

Samples were broken into small chips and only fresh pieces were selected for analyses. Selected chips for geochemical analyses were then cleaned with alcohol in an ultrasonic cleaner, then dried and crushed to fine powder (<200 mesh) using an automated agate mill. Importantly, a concerted effort was made to avoid direct contact with metal during all sample preparation procedures.

Major elements and TOC: Major elements and TOC analysis were carried out at ALS Chemex Lab (Aoshi, Guangzhou, China). Major elements were determined using X-ray fluorescence (XRF) spectrometry with a PANalytical Axios instrument. The analytical precision is generally better than 3%. TOC contents were analyzed using decarbonated material (carbonates were reacted with an excess of 50% HCl at 105°C to ensure decarbonation) by a LECO CS-844 analyzer. The precision was better than 0.1% based on the analysis of the GGC-09 standard.

Re-Os isotope analysis: Rhenium-osmium isotope analyses were carried out at the Metallogenic Chronology Lab at the IGGCAS, Beijing. About 0.5 g of fine powder from Mn carbonate ores was loaded into a Carius tube cooled in an ice-water

bath and treated with 2 mL HCl to release CO_2. Thereafter, 2 mL HCl, 6 mL HNO_3, along with the ^{185}Re-^{190}Os spike, were added to the Carius tube and reacted at 220°C for 48 h (Zhao et al., 2015). For the marlstone samples, 0.2 to 0.5 g power and a known amount of ^{185}Re-^{190}Os tracer solution were loaded in the Carius tube and treated with 8 mL CrO_3-H_2SO_4 solution (made from 0.25 g of CrO_3 per 1 mL of 4 *N* H_2SO_4) and then reacted at 220°C for 48 (Selby and Creaser, 2003).

Osmium was extracted as OsO_4 from the inverse aqua regia and CrO_3-H_2SO_4 solutions, respectively, by distillation in a steam bath (Jin et al., 2013), then trapped in 3 mL HBr, and ultimately purified by microdistillation. Osmium isotope ratios were measured by negative thermal ionization mass spectrometry (Thermo, Triton plus). The $^{187}Os/^{188}Os$ measurement was monitored by repeat analysis of the Johnson-Matthey standard from the University of Maryland (UMD) of 0.11378 ± 4 (2 SD, n = 20). After Os extraction, ethyl alcohol was added into the Re-bearing solution for 20 min to reduce Cr^{6+} completely to Cr^{3+}. Re was then purified by column chromatography using an anionic resin (AG1x8 100-200 mesh) (Morgan et al., 1995; Jin et al., 2013). Rhenium isotope ratios were determined by high resolution-inductively coupled plasma-mass spectrometry (HR-ICP-MS) (Thermo Fisher Element XR), used with mass fractionation corrected by the standard bracketing method. The average procedural blank for Re and Os in CrO_3-H_2SO_4 digestion was 44 ± 5 pg and 313 ± 154 fg, respectively, with an average $^{187}Os/^{188}Os$ value of 0.51 ± 0.16 (2σ, n = 8). For the inverse aqua regia procedure, the blank was 4.5 ± 0.6 pg and 305 ± 101 fg for Re and Os, and $^{187}Os/^{188}Os$ was 0.46 ± 0.11 (2σ, n = 4). All uncertainties are determined through an error propagation of uncertainties in Re and Os mass spectrometer measurements, total blank abundances, spike calibrations, and ^{187}Re decay constant of $1.666e^{-11} \pm 5.165e^{-14}$ a^{-1} (Smoliar et al., 1996). The Re-Os isotope data is calculated with 2σ uncertainties for $^{187}Re/^{188}Os$, $^{187}Os/^{188}Os$, and associated error correlation function (rho) to regress the isochron line using Isoplot (Ludwig, 2012).

Results

The organic-rich marlstones are composed of carbonate and siliciclastic layers, with some intercalated organic matter laminae (Fig. 3A). The organic-poor marlstones mainly consist of a mud matrix and micritic calcite (20–30%), with minor, evenly dispersed subangular quartz grains (less than 5%) (Fig. 3B). By comparison, the massive Mn ores are primarily composed of microparticle Mn carbonate aggregates and minor alabandite intergrown with disseminated organic matter (Fig. 3C). SEM and EDS analyses indicate that the Mn carbonate aggregates are dominated by pure rhodochrosite, with little Ca, Mg, and Fe (Fig. 3D).

TOC, major elements, and Re-Os composition data for Mn carbonate ores and host rocks from the Ortokarnash Mn deposit are provided in Tables 1 and 2. Geochemical trends are shown in a stratigraphic context in Figure 4.

The Mn carbonate ores are characterized by high Mn_3O_4 abundances (>50 wt %), low Al_2O_3 (0.29–3.72 wt %; avg 1.31 wt %) and TOC (0.12–0.62 wt %) contents. By comparison, the marlstone samples have low MnO (0.14–1.65 wt %) but high Al (4.81–12.61 Al_2O_3 wt %; avg 9.93 wt %) and TOC (0.54–1.19 wt %) concentrations.

The Mn carbonate ores have Re and Os abundances of 0.10 to 5.35 and 0.25 to 0.51 ppb, respectively, together with $^{187}Re/^{188}Os$ and $^{187}Os/^{188}Os$ ratios of 0.98 to 73.15 and 0.81 to 1.19, respectively. Linear regression of the Re-Os data for these samples yields a Model 1 age of 320.3 ± 6.6 Ma (mean square of weighted deviates [MSWD] = 1.4, n = 10, 2σ) with an Os_i value of 0.7959 ± 0.0029 (Fig. 5A1). By contrast, the hanging-wall marlstones are characterized by higher Re concentrations (12.65–38.38 ppb) but similar Os abundances (0.24–0.60 ppb) relative to the Mn carbonate ores, resulting in higher $^{187}Re/^{188}Os$ ratios (234–536) in the former. The $^{187}Os/^{188}Os$ compositions range from 1.84 to 3.43. Accordingly, the regression of isotopic data yields a Model 3 isochron age of 316.3 ± 8.0 Ma (2σ, n = 6, MSWD = 8.4) with an Os_i value of 0.609 ± 0.049 (Fig. 5B). Rhenium and Os concentrations in the footwall marlstones are comparable to those in the hanging-wall marlstones, varying from 6.83 to 31.87 and 0.13 to 0.54 ppb, respectively. The $^{187}Re/^{188}Os$ ratios of the footwall marlstones range from 302 to 889 and show a linear covariation with their corresponding $^{187}Os/^{188}Os$ ratios (range: 2.1–5.1; Table 2). Linear regression of the Re-Os data yields a Model 3 age of 296 ± 32 Ma (MSWD = 554, Os_i = 0.66 ± 0.27, n = 7, 2σ; Fig 5C).

Discussion

The inverse aqua regia digestion method and the Mn carbonate ores

The digestion method is vital for obtaining precise and accurate Re-Os radiometric ages for sedimentary rocks (Ravizza et al., 1991). The CrO_3-H_2SO_4 digestion protocol is considered the ideal approach for minimizing incorporation of Re and Os from detrital materials into hydrogenous components to obtain a precise Re-Os age and a homogeneous Os_i for most sedimentary rocks (Selby and Creaser, 2003; Rooney et al., 2011; Kendall et al., 2013). In this study, an Re blank of 44 ± 5 pg from the CrO_3-H_2SO_4 method is likely to contribute less than 1% of the marlstone but up to 46% to the Mn carbonate ores (avg 18%). Therefore, the CrO_3-H_2SO_4 protocol is appropriate for the marlstones but not for Mn carbonates samples. Given low Re abundance of the Mn carbonate coupled with low Al_2O_3 (0.29–3.72 wt %; Table 1, Fig. 4), which is an indicator of clastic input (Maliva et al., 1999; Brumsack, 2006), the low Re blank for the inverse aqua regia digestion method (4.5 ± 0.6 pg) is reasonable for the treatment of Mn carbonate ores resulting in an only 0.1 to 5.85% Re blank correction (Table 2.).

By using the inverse aqua regia digestion method we obtained a Model 1 regression age of 320.3 ± 6.6 Ma (MSWD = 1.4) for the Mn carbonate ores. The MSWD value is close to the ideal value of ~1, suggesting that the scatter of the isochron age is only linked to the uncertainties of the individual data, and is not controlled by geologic factors (Ludwig, 2012). The Os_i values of 0.7959 ± 0.0029 are highly consistent and indicate that Os in Mn carbonate ores was contributed by a common component. Additionally, it is noted that Re contents of 0.10 to 5.35 ppb obtained by this method largely overlap with values for the upper continental crust (0.2–2.0 ppb) (Esser and Turekian, 1993; Peucker-Ehrenbrink and Jahn, 2001). The absence of a correlation between Al_2O_3 and Re abundances indicates that the possible dissolution of the detrital

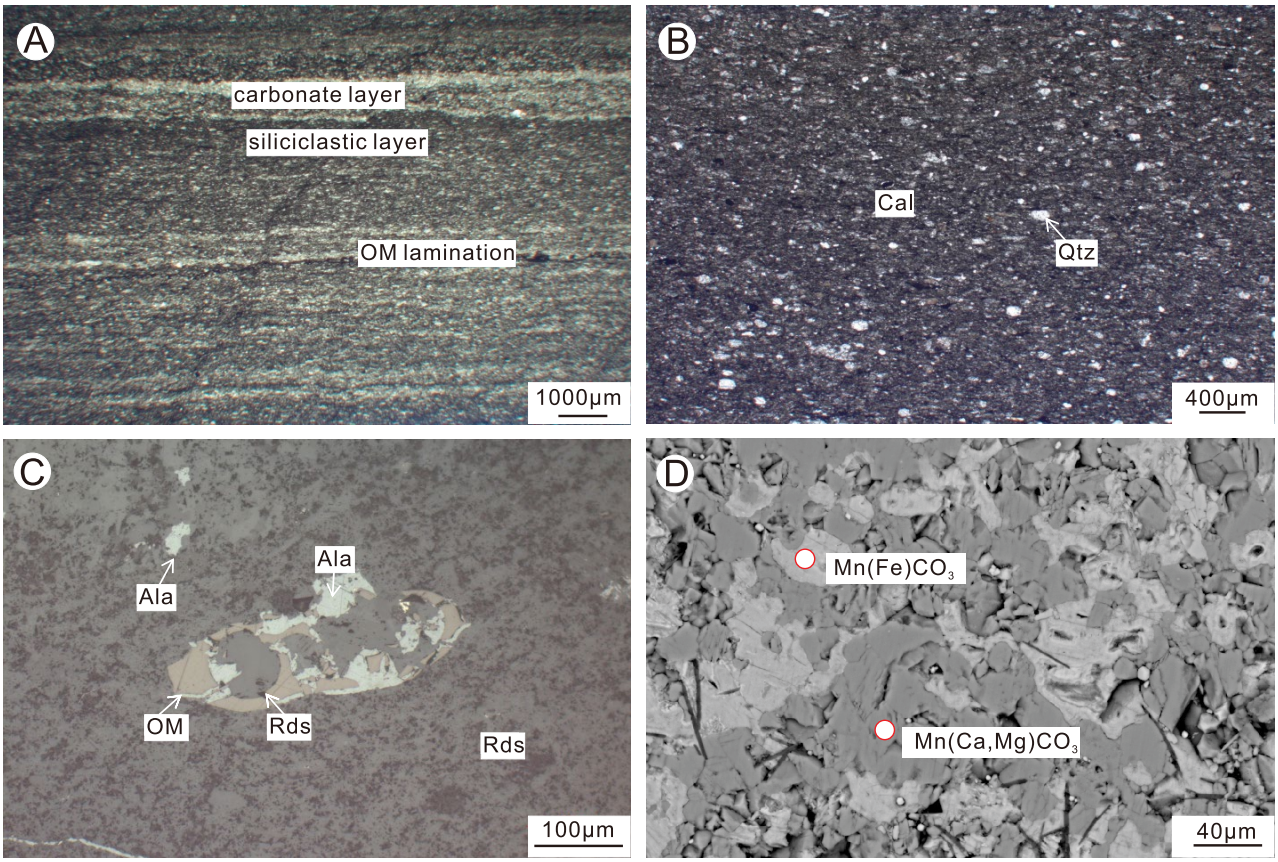

Fig. 3. Photomicrographs of the Mn-bearing sequence in Ortokarnash manganese deposit. (A) Organic-rich marlstone (Ort-93.6) showing the organic matter (OM) lamination intercalated within the carbonate and siliciclastic layers (plane-polarized light); (B) The organic-poor marlstone (Ort-81.0) is primarily composed of micritic calcite and minor evenly dispersed subangular quartz grains (plane-polarized light); (C) The Mn ore (Ort-87.3) showing alabandite intergrown with disseminated organic matter flakes within the Mn carbonate aggregates (reflected light); (D) Mn carbonate aggregates as dominate pure rhodochrosite, with little Ca, Mg, and Fe (backscattered electron image). Abbreviations: Ala = alabandite, Cal = calcite, Qtz = quartz, Rds = rhodochrosite.

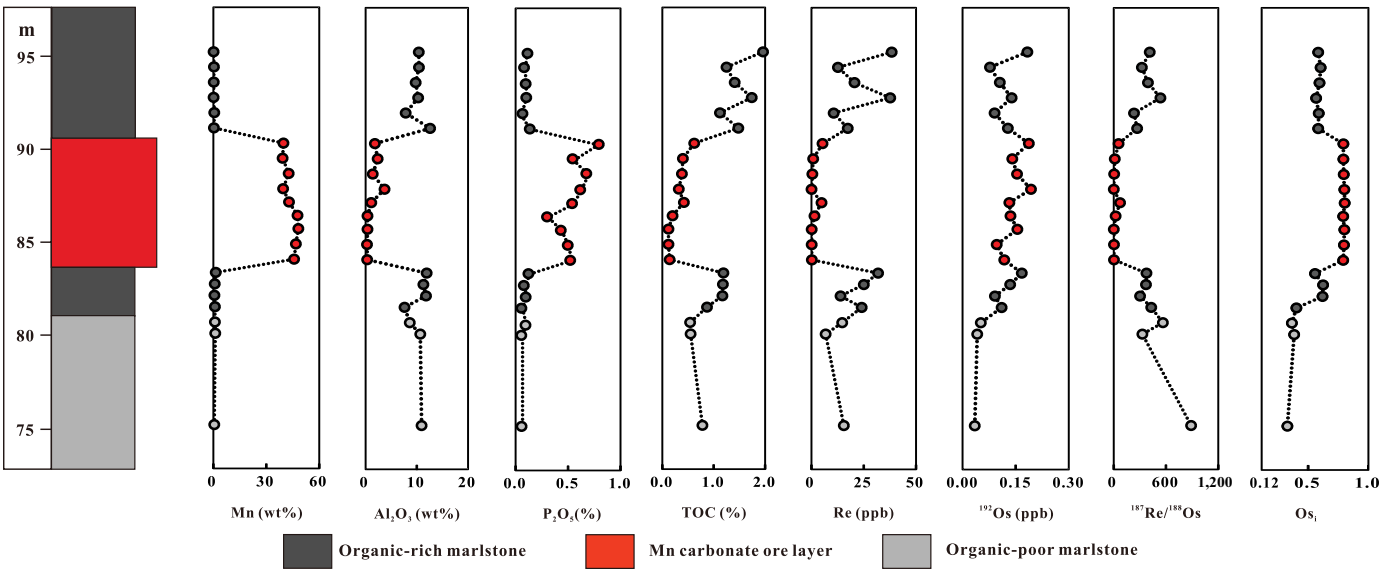

Fig. 4. Stratigraphic variations of the studied elements (Mn, Al, Re, P, and ^{192}Os), TOC, $^{187}Re/^{188}Os$, and Os_i composition according to Tables 1 and 2.

Table 1. Major Elements and Total Organic Carbon (TOC) Concentrations (wt %) for the Mn Carbonate Ores and Hosted Marlstone Samples in the Ortokarnash Manganese Ore Deposit

Sample	Type	Depth/m	TOC (wt %)	SiO_2	TiO_2	Al_2O_3	TFe_2O_3	MnO/Mn_3O_4	CaO	MgO	K_2O	Na_2O	P_2O_5	SO_3	LOI	Total
Hanging wall																
Ort-95.2	Organic-rich marlstone	95.2	1.96	52.3	0.39	10.4	4.06	0.10	12.8	1.60	0.60	3.35	0.11	4.11	11.8	101.7
Ort-94.4	Organic-rich marlstone	94.4	1.25	48.5	0.38	10.4	4.80	0.37	13.9	2.58	1.22	2.04	0.09	3.83	12.8	101.0
Ort-93.6	Organic-rich marlstone	93.6	1.41	48.6	0.36	9.78	4.20	0.24	15.2	1.78	1.02	2.34	0.10	3.78	13.6	100.9
Ort-92.8	Organic-rich marlstone	92.8	1.74	49.2	0.41	10.3	4.55	0.12	14.3	1.46	0.44	3.29	0.10	4.85	11.5	100.5
Ort-92.0	Organic-rich marlstone	92.0	1.12	57.2	0.28	7.83	3.70	0.65	12.0	2.11	1.08	0.96	0.05	3.59	10.8	100.2
Ort-91.2	Organic-rich marlstone	91.2	1.48	54.6	0.42	12.6	4.23	0.42	9.11	2.64	1.71	1.84	0.13	2.90	9.84	100.4
Mn ore bed																
Ort-90.4	Mn carbonate ore	90.4	0.62	4.25	0.08	1.81	0.90	55.5	2.96	2.65	<0.01	<0.01	0.79	0.05	30.8	99.8
Ort-89.6	Mn carbonate ore	89.6	0.40	9.83	0.09	2.38	1.74	54.9	1.46	4.25	<0.01	<0.01	0.56	1.07	24.0	100.3
Ort-88.8	Mn carbonate ore	88.8	0.38	6.50	0.06	1.40	0.95	59.7	1.59	2.97	<0.01	<0.01	0.70	0.87	26.0	100.8
Ort-88.0	Mn carbonate ore	88.0	0.32	9.18	0.11	3.72	1.55	55.3	1.08	4.65	<0.01	<0.01	0.63	0.12	23.0	99.3
Ort-87.3	Mn carbonate ore	87.3	0.42	6.96	0.02	1.11	1.11	60.0	1.40	2.06	<0.01	<0.01	0.55	0.74	25.9	99.8
Ort-86.6	Mn carbonate ore	86.6	0.20	5.68	<0.01	0.37	2.08	66.7	0.88	2.02	<0.01	0.01	0.31	0.75	20.5	99.2
Ort-85.9	Mn carbonate ore	85.9	0.12	2.84	<0.01	0.37	0.64	67.4	1.76	2.42	<0.01	0.03	0.44	0.05	24.3	100.3
Ort-85.1	Mn carbonate ore	85.1	0.12	2.96	<0.01	0.29	0.64	65.4	1.77	2.29	<0.01	0.01	0.51	0.07	25.2	99.1
Ort-84.3	Mn carbonate ore	84.3	0.14	2.85	<0.01	0.31	0.52	64.0	1.81	2.18	<0.01	<0.01	0.53	0.10	26.9	99.1
Footwall																
Ort-83.6	Organic-rich marlstone	83.6	1.19	50.7	0.43	11.9	5.36	1.65	8.94	3.82	1.00	2.71	0.13	7.40	5.55	99.6
Ort-83.0	Organic-rich marlstone	83.0	1.18	50.6	0.4	11.3	4.14	0.97	11.7	2.24	1.41	2.39	0.08	5.23	10.5	100.8
Ort-82.4	Organic-rich marlstone	82.4	1.17	51.9	0.44	11.8	5.95	0.74	9.56	2.49	1.87	1.66	0.10	8.42	5.38	100.3
Ort-81.8	Organic-poor marlstone	81.8	0.87	51.8	0.28	7.62	2.32	1.14	15.9	1.40	0.74	2.13	0.06	2.73	13.6	99.7
Ort-81.0	Organic-poor marlstone	81.0	0.54	40.4	0.37	8.62	6.84	1.13	15.5	9.48	0.02	0.28	0.10	3.40	14.3	100.4
Ort-80.4	Organic-poor marlstone	80.4	0.55	33.8	0.22	10.7	6.12	1.34	19.8	4.88	0.70	1.96	0.06	1.56	18.4	99.5
Ort-75.6	Organic-poor marlstone	75.6	0.78	37.3	0.45	10.9	7.64	0.60	16.4	4.01	0.70	3.43	0.06	8.98	10.1	100.6

Notes: Mn concentrations of Mn carbonate ore samples are presented in the form of Mn_3O_4; hosted marlstone samples are in the form of MnO

Table 2. Re-Os Isotope Data for the Mn Carbonate Ores and Hosted Marlstone Samples in Ortokarnash Manganese Ore Deposit

Sample	Re (ppb)	Os (ppb)	^{192}Os (ppb)	^{187}Re/^{188}Os	^{187}Os/^{188}Os	rho	Re Blank (%)	^{188}Os Blank (%)	^{187}Os Blank (%)	Os_i
Hanging wall										
Ort-95.2	38.38 ± 0.05	0.6013 ± 0.0009	0.1830 ± 0.0004	414.7 ± 1.0	2.801 ± 0.006	0.779	0.23	0.03	0.01	0.603 ± 0.002
Ort-94.4	12.65 ± 0.05	0.2430 ± 0.0009	0.0775 ± 0.0004	323.0 ± 2.0	2.330 ± 0.012	0.696	0.68	0.08	0.02	0.619 ± 0.005
Ort-93.6	20.62 ± 0.05	0.3420 ± 0.0009	0.1052 ± 0.0004	392.8 ± 1.7	2.694 ± 0.010	0.779	0.42	0.06	0.01	0.612 ± 0.003
Ort-92.8	37.67 ± 0.12	0.4841 ± 0.0016	0.1387 ± 0.0007	536.7 ± 3.0	3.435 ± 0.016	0.780	0.39	0.03	0.00	0.591 ± 0.004
Ort-92.0	10.68 ± 0.05	0.2689 ± 0.0010	0.0904 ± 0.0004	234.1 ± 1.6	1.839 ± 0.010	0.554	0.82	0.07	0.02	0.599 ± 0.005
Ort-91.2	17.37 ± 0.06	0.3882 ± 0.0009	0.1279 ± 0.0004	268.8 ± 1.2	2.020 ± 0.006	0.600	0.51	0.05	0.01	0.595 ± 0.003
Mn ore bed										
Ort-90.4 [1]	5.353 ± 0.009	0.5128 ± 0.0006	0.1874 ± 0.0002	56.65 ± 0.11	1.095 ± 0.008	0.095	0.10	0.05	0.02	0.792 ± 0.006
Ort-89.6 [1]	0.8818 ± 0.0035	0.3741 ± 0.0004	0.1407 ± 0.0002	12.44 ± 0.05	0.858 ± 0.008	0.040	0.64	0.07	0.04	0.792 ± 0.008
Ort-88.0 [1]	0.4759 ± 0.0033	0.4083 ± 0.0004	0.1541 ± 0.0002	6.130 ± 0.043	0.829 ± 0.005	0.019	1.18	0.06	0.04	0.796 ± 0.007
Ort-88.8 [1]	0.0957 ± 0.0031	0.5109 ± 0.0005	0.1933 ± 0.0002	0.983 ± 0.032	0.806 ± 0.006	0.004	5.85	0.05	0.03	0.801 ± 0.027
Ort-87.3 [1]	4.871 ± 0.012	0.3655 ± 0.0005	0.1321 ± 0.0002	73.15 ± 0.20	1.194 ± 0.009	0.096	0.12	0.07	0.03	0.803 ± 0.006
Ort-86.6 [1]	1.524 ± 0.005	0.3620 ± 0.0004	0.1353 ± 0.0002	22.35 ± 0.08	0.911 ± 0.008	0.050	0.37	0.07	0.04	0.791 ± 0.008
Ort-85.9 [1]	0.1651 ± 0.0031	0.4088 ± 0.0005	0.1546 ± 0.0002	2.119 ± 0.040	0.811 ± 0.007	0.009	3.37	0.06	0.04	0.800 ± 0.017
Ort-85.1 [1]	0.1356 ± 0.0031	0.2544 ± 0.0013	0.0962 ± 0.0005	2.798 ± 0.066	0.812 ± 0.022	0.043	4.12	0.10	0.06	0.797 ± 0.029
Ort-85.1_rept[1]	0.1312 ± 0.0031	0.2492 ± 0.0007	0.0943 ± 0.0003	2.761 ± 0.066	0.809 ± 0.020	0.014	4.30	0.10	0.06	0.795 ± 0.027
Ort-84.3 [1]	0.2091 ± 0.0031	0.3115 ± 0.0004	0.1178 ± 0.0002	3.522 ± 0.053	0.810 ± 0.007	0.012	2.69	0.08	0.05	0.791 ± 0.014
Footwall										
Ort-83.6	31.87 ± 0.05	0.5379 ± 0.0010	0.1675 ± 0.0004	376.3 ± 1.1	2.568 ± 0.007	0.728	0.28	2.35	0.01	0.538 ± 0.002
Ort-83.0	25.10 ± 0.06	0.4324 ± 0.0009	0.1342 ± 0.0004	370.0 ± 1.4	2.602 ± 0.008	0.706	0.35	2.31	0.01	0.606 ± 0.003
Ort-82.4	13.95 ± 0.05	0.2835 ± 0.0009	0.0913 ± 0.0004	302.3 ± 1.7	2.235 ± 0.009	0.702	0.62	1.89	0.01	0.604 ± 0.004
Ort-81.8	24.04 ± 0.08	0.3594 ± 0.0009	0.1104 ± 0.0004	430.6 ± 2.1	2.704 ± 0.009	0.674	0.36	2.69	0.01	0.382 ± 0.002
Ort-81.0	14.71 ± 0.05	0.1787 ± 0.0009	0.0514 ± 0.0004	565.5 ± 4.6	3.388 ± 0.026	0.855	0.60	3.54	0.02	0.337 ± 0.004
Ort-80.4	6.831 ± 0.045	0.1263 ± 0.0009	0.0411 ± 0.0004	329.2 ± 3.7	2.142 ± 0.019	0.797	1.29	2.06	0.03	0.367 ± 0.005
Ort-75.6	15.51 ± 0.08	0.1383 ± 0.0015	0.0344 ± 0.0006	889.3 ± 16.5	5.081 ± 0.092	0.952	0.95	5.58	0.01	0.282 ± 0.007

All uncertainties are given as 2σ, including the uncertainties of measurement, blank plus spike calibrations; rho is the associated error correlation; Os_i is the initial ^{187}Os/^{188}Os isotope ratio calculated at 316.3, 320.3, and 322.9 Ma for each unit, respectively; rept = replicate analysis of the same powder

[1] Inverse aqua regia digestion was used for Mn ore carbonate samples, whereas CrO_3-H_2SO_4 digestion was applied for unmarked marlstone samples

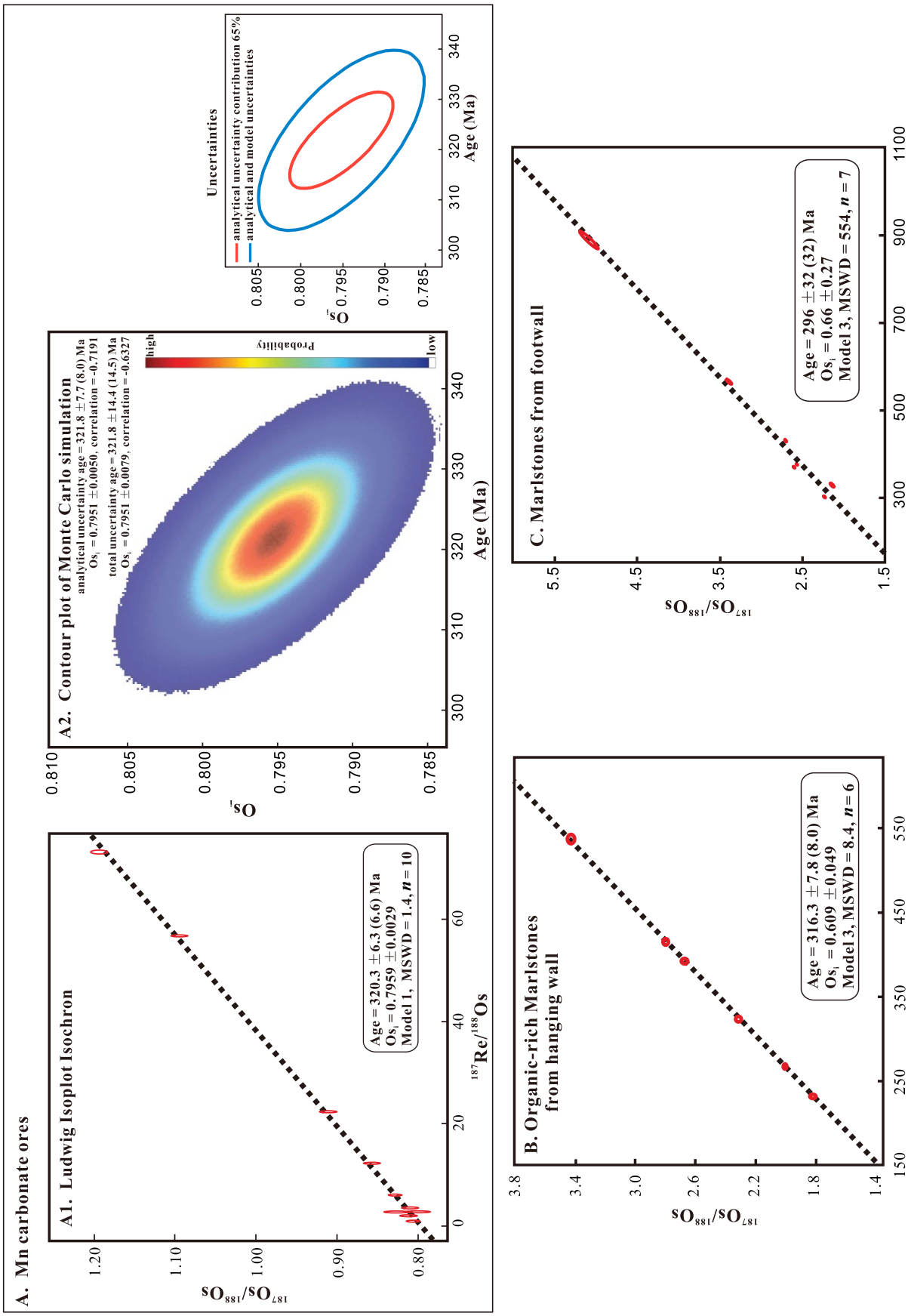

Fig. 5. Re-Os geochronologic results for the Mn carbonate ores (A), hanging-wall marlstones (B), and footwall marlstones (C) in the Ortokarnash Mn deposit. The Re-Os isotope data, including the 2σ calculated uncertainties for $^{187}Re/^{188}Os$ and $^{187}Os/^{188}Os$ and the associated error correlation function (rho), are regressed to yield a Re-Os date using Isoplot v.4.15 (A1, B, and C; Ludwig, 2003). The Mn carbonate ore samples are also regression calculated using a Monte Carlo approach (A2, Li et al., 2019), which consists of a Monte Carlo age simulation contour plot and Monte Carlo results of the analytical only and analytical + model uncertainties obtained from Monte Carlo simulation at the 2-sigma level. Bracketed age uncertainties include the uncertainty of the decay constant. MSWD = mean square of weighted deviates.

fraction by inverse aqua regia has an insignificant influence on our analysis. In summary, our results confirm that the inverse aqua regia digestion is a potential approach to dissolve Mn carbonate ores for Re-Os analysis.

Re-Os geochronology of the Ortokarnash Mn carbonate deposit

Samples from the ~6-m-thick ore interval yield a Re-Os age of 320.3 ± 6.6 Ma (Model 1, MSWD = 1.4; Fig. 5A1). Given the consistent results over this thickness, we interpret this as the mineralization age of the Ortokarnash Mn carbonate deposit, and therefore this age represents the first time a Mn carbonate ore has successfully been dated using Re-Os isotope analysis. The uncertainty that arises from the Model 1 fit is always underestimated and does not incorporate geologic uncertainties into the age uncertainties (Li et al., 2019). The Monte Carlo method, however, propagates uncertainties (2σ) from both analytical measurements and model assumptions in a consistent manner irrespective of the probability of fit (Li et al., 2019). With both uncertainties, collectively termed total uncertainty, an age of 321.8 ± 14.5 Ma and Os_i value of 0.7951 ± 0.0079 are calculated using the beta version of the Isochron program (see Fig. 5A2; Li et al., 2019). The Monte Carlo results suggest that analytical uncertainty accounts for about 65% of the age uncertainty and 63% of the Os_i uncertainty (Fig. 5A2). Owing to the highly homogeneous Os_i value yielded in both fitting approaches, we interpret this large age uncertainty (4.5%, 2σ) to be the result of limited spread in the $^{187}Re/^{188}Os$ value (1–73). The limited range of low $^{187}Re/^{188}Os$ ratios is likely related to variable redox conditions during Mn carbonate mineralization, leading to low Re and relatively high Os (see next section).

This newly obtained Re-Os age for Mn carbonate ore samples from the Ortokarnash Mn deposit agrees well with a recent U-Pb zircon age (322.9 ± 1.8 Ma [Zhang, 2020]) from the volcanic breccia-bearing limestone that conformably underlies the calcareous mudstones by ~65 m and provides a robust, maximum depositional age constraint on the Mn carbonate (Fig. 2). Regionally, the limited zircon U-Pb ages from the basalts of Wuluate Formation, which unconformably underlies the ore-bearing Kalaatehe Formation, yield $^{206}Pb/^{238}U$ ages of 326.6 ± 1.3, 327.3 ± 2.6, and 331.5 ± 1.5 Ma (Gao et al., 2018), suggesting that the Kalaatehe Formation is younger than ~326 Ma. In the absence of geochronological dates, the overlying Maerkanque-Kusaishan Formation is considered to have been deposited in the lower Permian based on the observed fusulinds *Dunbarinella sp.* and brachiopods *Stenoscisma sp.* fossil occurrences (Gao, 2015). These constraints place deposition of the Kalaatehe Formation between 326 and 300 Ma, which is fully consistent with the Re-Os age of Mn carbonate ores determined here. This good correlation between direct and indirect age constraints demonstrates that the Re-Os isotope system can be successfully applied to sedimentary Mn carbonate ores in order to provide robust, direct ore-forming ages that are needed to understand the genesis of these deposits.

In this sedimentary sequence, regression of hanging-wall marlstones yields a Model 3 age of 316.3 ± 8.0 Ma (MSWD = 8.6; Os_i = 0.609 ± 0.049, Fig. 5B), representing a minimum mineralization age for this deposit. The age uncertainty determined is considered to be controlled by the variation in individual Os_i ratios, which range from 0.591 to 0.619 when calculated at 316.3 Ma. Furthermore, the imprecise Re-Os age (296 ± 32 Ma; MSWD = 554; Fig. 5C) from the footwall marlstone samples is considered to relate to the variation in Os_i values (0.66 ± 0.27). The variation in Os_i values suggests that either fluctuations in the balance and/or flux of Os inputs or alteration prior to Mn mineralization. Additionally, sampling from a large stratigraphic interval of ~8 m is also likely to increase variations in Os_i. Despite this expanded uncertainty, the Re-Os isotope age is consistent, within uncertainty, with that of the Mn carbonate ores and hanging-wall marlstone. Significantly, we demonstrate that Re-Os geochronology is an effective way to directly date Mn carbonate ores.

Re and Os uptake and fractionation in Ortokarnash Mn carbonate ores

Rhenium and Os in marine black shales can exhibit positive correlations with TOC contents (Rooney et al., 2010). In this study, the Re shows a strong correlation with TOC for both hanging-wall marlstones (R^2 = 0.91) and Mn ores (R^2 = 0.57) (Fig. 6A), indicating that Re was likely incorporated into the Mn ores and sediments along with the organic matter. Further, it has been shown that Mg can largely suppress Re absorption by TOC in the water column (Miller et al., 2011), and as such, the correlation of Re versus TOC + 1/MgO is favored. Using this method, we obtain a strong linear relationship with R^2 = 0.91 (Fig. 6B) for the ore samples and marlstones (R^2 = 0.98; Fig. 6B), confirming that Re uptake is dominated by organic matter for the Mn carbonate ores as well as the marlstone samples. On the other hand, the poor correlation between Os and TOC contents for Mn carbonate ores (R^2 = 0.36, Fig. 6C) contrasts with that of hanging-wall marlstones (R^2 = 0.91, Fig. 6C), suggesting different chelation mechanisms from Re. As noted above, these results indicate that Re is strongly associated with the organic matter, while Os may not be as tightly controlled by organic matter abundance in Mn carbonate ores.

The enrichment of Re and Os in sediments is also controlled by the redox conditions of the depositional environment (Dubin and Peucker-Ehrenbrink, 2015; Lu et al., 2017). Rhenium, a redox-sensitive trace metal, behaves conservatively in oxygenated conditions and is prone to being enriched in sediments that are anoxic or overlain by an anoxic water column (Sheen et al., 2018), whereas Os removal can take place under a range of water column redox conditions (Yamashita et al., 2007; Sheen et al., 2018). As indicated by previous studies (Calvert and Pedersen, 1996; Johnson et al., 2016), the deposition of Mn carbonate in the sediment normally requires two steps, each occurring under distinct redox conditions. Briefly, Mn(II) is first oxidized to form Mn(IV) oxyhydroxides in seawater via abiotic (Huckriede and Meischner, 1996; Yu et al., 2016) and/or biotic (Tebo et al., 2004) oxidation. The Mn(IV) oxyhydroxides are then diagenetically converted to Mn(II) carbonates in anoxic pore water through the coupled oxidation of organic matter (Thamdrup et al., 2000; Kristin et al., 2013).

During the first stage of Mn(II) oxidation, Re would mainly be present in the form of ReO_4^- in oxic seawater (Anbar et al., 1992) and is decoupled from the Mn(IV) oxyhydroxides

(Colodner et al., 1993; Crusius et al., 1996; Sheen et al., 2018). This results in low concentrations of Re associated with the Mn(IV) oxyhydroxide precipitates. By comparison, the soluble $OsCl_6^{2-}$, which is readily subjected to hydrolysis and absorbed onto mineral surfaces, tends to concentrate on Mn(IV) oxyhydroxide precipitates (Burton et al., 1999; Yamashita et al., 2007). Hence, modern ferromanganese crusts and Mn nodules that are formed by Mn(II) oxidation are generally characterized by high Os but low Re abundances (Burton et al., 1999; Peucker-Ehrenbrink and Ravizza, 2000; McDaniel et al., 2004). This pattern is also observed in the Mn carbonate ores of the Ortokarnash deposit presented here.

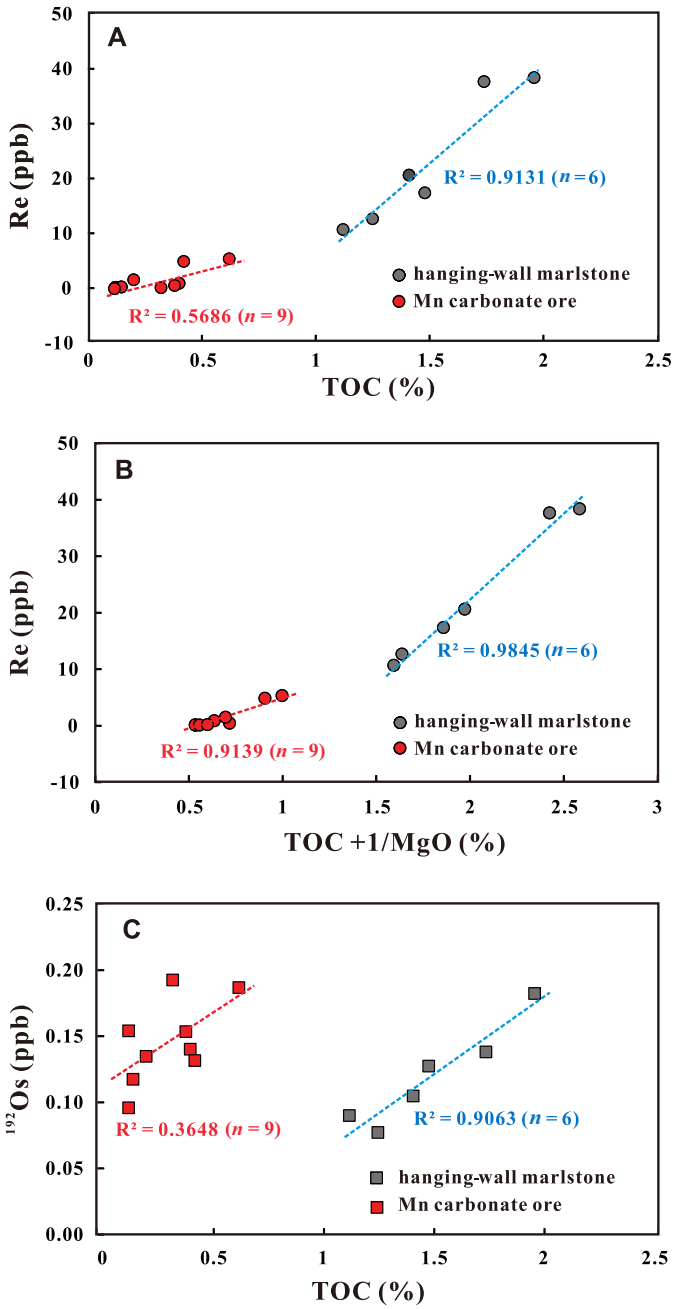

Fig. 6. Covariation between (A) Re abundance and total organic carbon (TOC), (B) Re abundance and TOC + 1/MgO, and (C) ^{192}Os abundance and TOC are shown. Red dashed lines represent Mn carbonate ore samples and blue dashed lines represent hanging-wall marlstones, respectively.

During diagenesis, Mn(IV) oxyhydroxides are commonly reduced to dissolved Mn(II) in the presence of organic matter in anoxic pore waters leading to the precipitation of Mn(II) carbonates (Konhauser, 2007; Johnson et al., 2016). Considering that dissolved Re(VII) is scavenged by organic complexes under anoxic conditions in the form of insoluble Re(IV) (Morford et al., 2005), its enrichment in the sediments can occur when there is an abundant reductant available. Notably, as Mn(IV) oxyhydroxides have a higher electrode potential than Re(VII) (Johnson et al., 2016; Dickson et al., 2020), it preferentially reacts with organic matter. In other words, the presence of excess organic matter in the sediments is likely to be a prerequisite for the subsequent enrichment of Re in Mn carbonates during diagenesis, because on one hand organic matter may prevent the oxidation of Re(IV) by Mn(IV) oxyhydroxides, and on the other hand the surplus organic matter may chelate Re(IV) during authigenic Mn carbonate formation. The above discussion is in line with the observed positive correlation between the amount of residual organic matter and Re abundances in the Mn carbonate ores (Fig. 6A, B).

The enrichment process of Os in Mn carbonates during diagenesis is not yet fully understood. The weak relationship exhibited between ^{192}Os and TOC in Mn carbonate ores (R^2 = 0.36, Fig. 6C) suggests that Os released by Mn(IV) oxyhydroxides in the early stages of diagenesis is not completely absorbed by TOC, and may be partly inherited by self-generated Mn carbonate and authigenic sulfides such as alabandite (Yamashita et al., 2007). As mentioned above, Os fixation is closely related to and controlled by Mn(II) oxidation in the water column. We suggest that the absorbed Os would be released to the pore waters during the reduction of Mn(IV) oxyhydroxides, and subsequently be captured during the precipitation of authigenic Mn(II) carbonates. Therefore, it is highly possible that the Os in our Mn carbonate ores is inherited from the Mn(IV) oxyhydroxide precursors where the initial Os components were adsorbed from coeval seawater (McDaniel et al., 2004; Klemm et al., 2005).

The different chelating mechanism coupled with variable redox conditions during Mn carbonate mineralization seems to be the cause of the limited spread in the observed low $^{187}Re/^{188}Os$ ratios. Still, remnant organic matter in the Ortokarnash Mn carbonate ores would have captured and preserved Re during authigenic Mn carbonate formation. As a result, these deposits have the potential to allow for the direct dating of mineralization by Re-Os. At the same time, the preservation of seawater Os via the adsorption to the Mn(IV) oxyhydroxide precursors provides a unique snapshot into the isotopic compositions (Os_i) at the time of deposition, thereby providing insights into the paleomarine environmental conditions during Mn ore deposition.

Implications for the genesis of the Ortokarnash Mn carbonate ores

The Os_i ratio derived from the hydrogenous fraction of sedimentary rocks has long been considered to reflect the seawater Os isotope composition contemporaneous to deposition (Ravizza and Turekian, 1989, 1992; Ravizza et al., 1991). Since those early studies, large variations in seawater $^{187}Os/^{188}Os$

compositions through time have been revealed by analyzing various marine sediments, including hydrogenic Fe-Mn crust, organic-rich mudrock, and oxic pelagic sediment (Paquay et al., 2014; Josso et al., 2019; Rooney et al., 2020). These variations are proposed to reflect changes in the balance between radiogenic and unradiogenic Os input fluxes to seawater. The principal radiogenic Os source ($^{187}Os/^{188}Os$ ~1.4) is riverine input derived from the continental crust; possible sources of unradiogenic Os ($^{187}Os/^{188}Os$ ~0.12) include the hydrothermal alteration of ultramafic rocks and the dissolution of cosmic dust (Allègre and Luck, 1980; Oxburgh, 1998; Sharma et al., 2000). Collectively, it is reasonable to assume that variations in seawater Os isotope compositions are related to and controlled by changes in the relative contributions of these isotopically distinct sources.

As shown in Figure 4, our isochron age for hanging-wall marlstones from the Ortokarnash Mn deposit returned Os_i values of 0.609 ± 0.049. This value is similar to the initial ratio of 0.55 ± 0.02 at 317 ± 2 Ma for the contemporary black shales in West Virginia, USA (see Tripathy et al., 2015). Considering there is no evidence to support a connection between these two basins at the Mississippian-Pennsylvanian boundary (Yin and Harrison, 2000), we tentatively suggest that the $^{187}Os/^{188}Os$ value of ~0.6 represents the Os isotope composition of global seawater at ~320 Ma, which is also supported by the identical initial ratios of 0.54 to 0.61 (calculated at 323 Ma) for three footwall marlstones neighboring the Mn ores. On the other hand, it is noted that the calculated Os_i ratios of all seven footwall marlstone samples increase from 0.28 to 0.61 in an ascending order. In this respect, the critical question becomes, how did seawater in the Ortokarnash basin generate such low $^{187}Os/^{188}Os$ values (0.28–0.38) during the deposition of the footwall marlstones and, crucially, why did the Os_i of the Ortokarnash basin increase from 0.28 to 0.61?

The significantly lower Os_i values for the lower interval of the footwall marlstones indicates that the Os influx to the Ortokarnash basin at that time was dominated by an unradiogenic input, likely from a mantle-derived source. In other words, it is likely that submarine volcanism and related hydrothermal vents as well as the halmyrolysis of the underlying basalts, which tend to have low $^{187}Os/^{188}Os$ ratios, were the dominant Os source to the basinal water. This conclusion is supported by the presence of volcanic breccia in the Member 1 limestone of the Kalaatehe Formation that underlies the studied samples (Zhang et al., 2020). Moreover, mafic to intermediate volcanic rocks (326–327 Ma) have been widely identified in the Wuluate Formation, thus indicating the development of extensive volcanism prior to regional carbonate sedimentation (Fig. 7A). Accordingly, the increasing $^{187}Os/^{188}Os$ ratios of the water column, as indicated by increasingly radiogenic Os_i values for footwall marlstones (Fig. 4), likely reflects the diminished supply of unradiogenic Os to the Ortokarnash basin during volcanic quiescence or weakened basalt halmyrolysis once capped with a carbonate succession (Fig. 7B). Furthermore, rock assemblages of the Upper Kalaatehe Formation are indicative of a transgression event, with the manganese deposition occurring during the highstand systems tract (Zhang et al., 2020). During the transgression, the relative rise in sea level would lead to an increase in the seawater component within the basin (with a $^{187}Os/^{188}Os$ value of ~0.6), which would accelerate mixing with global seawater. In turn, this would result in the masking of Os isotope signatures from earlier volcanism and moving the basin's Os isotope composition toward that of global seawater (Fig. 7B).

In comparison to the footwall marlstones, the isochron-derived Os_i ratio of Mn carbonate ores rose abruptly and significantly to a relatively homogeneous value of 0.7959 ± 0.0029 (Fig. 4). This value is higher than that expected for global seawater (~0.6) recorded by the underlying marlstone. As discussed above, the Os_i ratios of the Mn carbonate ores were inherited from the Mn(IV) oxyhydroxide precursors, which obtained their Os isotope compositions through the adsorption of Os in the water column. Thus, the observed increase in these ore samples indicates that the seawater $^{187}Os/^{188}Os$ value must have risen significantly during the deposition of the Mn(IV) oxyhydroxides. Considering that the riverine input is the main radiogenic Os source, which possesses an $^{187}Os/^{188}Os$ ratio of ~1.4, we conclude that the elevated Os_i values for the Ortokarnash Mn carbonate ores were caused by an increasing supply of radiogenic Os from continental runoff.

Enhanced riverine Os input was likely the result of increased chemical weathering and/or riverine supply. During the late Carboniferous (ca. 320 Ma), the rapid expansion of paleotropical land plants, and vascular land plants in particular (Cleal and Thomas, 2005; Goddéris et al., 2017; Chen et al., 2018), would have enhanced the soil CO_2 inventory and led to an increase in the chemical weathering of the continents (Tripathy et al., 2015). In addition, the Ortokarnash Mn carbonate deposit was formed during the Late Paleozoic ice age (~340–285 Ma), and to be exact, approximately coincides with the end of the Serpukhovian-Bashkirian glaciation (319.57 ± 0.086 Ma) (Gulbranson et al., 2010). Hence, it is possible that the profound effect was caused by this paleoclimatic event, such that an increased supply from continental runoff and/or a shift in the style of fluvial channels (Finlay et al., 2010), could have led to the increased riverine Os input at this time.

Significantly, the $^{187}Os/^{188}Os$ ratio returns to the global seawater value of ~0.6 following deposition the Ortokarnash deposit, as evidenced by the Os_i value of the hanging-wall marlstones (0.609 ± 0.049, Fig. 5). This suggests the cessation of enhanced riverine input to the basin. This hypothesis matches well with the classic Baltic Sea model, where a large number of Mn carbonate layers formed following the injection of oxygenated inflows of denser water from the North Sea to the Baltic Sea (Huckriede and Meischner, 1996; Dellwig et al., 2018; Häusler et al., 2018). Following this model, it can be inferred that the riverine waters, enriched in O_2, mixed with seawater to disturb and lower the Mn(III/IV)/Mn(II) redoxcline. In this regard, we propose that both the enhanced mixing of O_2-enriched river water and sea level rise coinciding with the transgression facilitated interactions between dissolved Mn(II) and O_2, and thus promoted the deposition of Mn(IV) oxyhydroxide precursors along the slope of the basin. Moreover, it should also be noted that both elevated riverine influx and upwelling associated with the transgression would have provided abundant nutrients to the surface waters, as evidenced by relatively high P_2O_5 abundances in the Mn carbonate ores (avg 0.56%; Table 1, Fig. 4) relative to the associated marlstones (avg 0.09%), leading to an increase

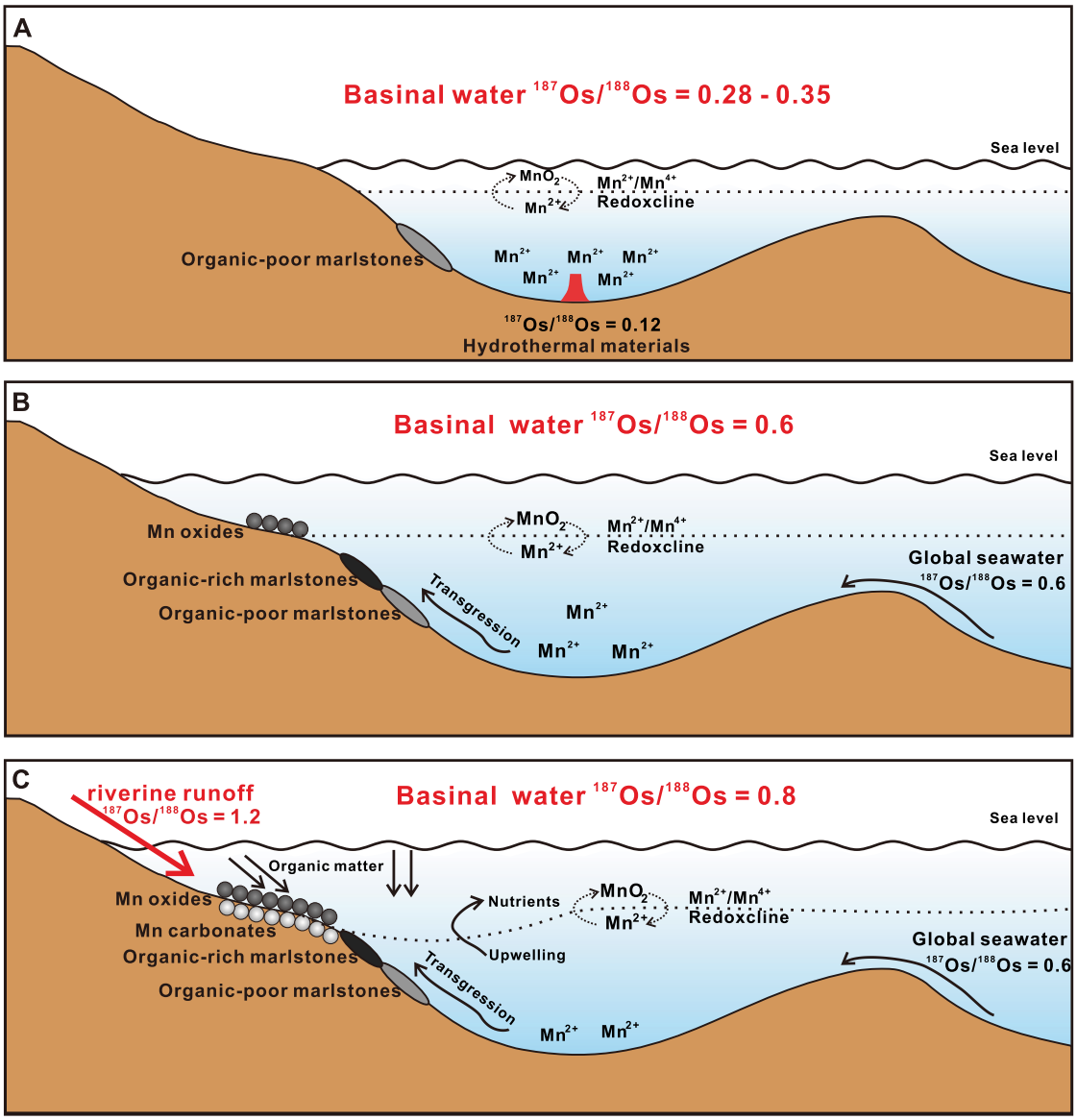

Fig. 7. Model for deposition of Mn minerals during the late Carboniferous (~320 Ma) leading to the formation of the Ortokarnash Mn carbonate deposit (modified from Zhang et al., 2020), based on variations in the Os_i of basinal seawater. (A) Os_i = 0.28-0.35; initially a high abundance of hydrothermal inputs results in a low Os_i in the basin. (B) Os_i = 0.6; a transgression brings in more seawater and accelerates the mixing process between basinal seawater and the global ocean. (C) Os_i = 0.8; enhanced riverine input during the transgression process creates conditions favorable for the Mn mineralization formation, including the input of oxygenated riverine water that promotes Mn(II) oxidation. This influx of continental runoff and global seawater also brings nutrients into the basin, leading to increased primary productivity and organic matter deposition, which in turn promotes the diagenetic production of Mn(II) carbonates in the sediments.

in primary productivity and consumption of dissolved O_2 in the water column. The subsequent burial of excess organic matter, together with Mn(IV) oxyhydroxides, in turn, would have created conditions favorable for the formation of authigenic Mn(II) carbonates during diagenesis (Fig. 7C) (Marin and Giresse, 2001; Neumann et al., 2002; Meister et al., 2009; Zhang et al., 2020). In summary, we suggest that enhanced riverine input during the transgression is an important factor for Mn mineralization in the Ortokarnash area, although more detailed paleogeographic data are needed to further test our model.

Conclusions

This study confirms the potential for the Re-Os system to be applied as a geochronometer for constraining mineralization ages and processes for sedimentary Mn carbonate deposits. Following the inverse aqua regia digestion method, the Re-Os age obtained here for the Mn carbonate ores of the Ortokarnash Mn deposit is indistinguishable, within analytical uncertainty, from the youngest detrital zircon U-Pb age of the underlying volcanic breccia-bearing limestone and the Re-Os depositional age of the overlying marlstone. This provides a

strong case for Re-Os geochronology of Mn carbonate ores as a viable tool for constraining their mineralization ages.

In addition, Re-Os systematics of the Mn carbonate ores provide an important glimpse into the Re and Os cycle, as well as changes in basinal water initial $^{187}Os/^{188}Os$ values contemporaneous to the deposition of the Ortokarnash Mn deposit. We suggest that Re was preferentially enriched in the organic matter residue and retained following the diagenetic reduction of the Mn(IV) oxyhydroxide precursors in suboxic or anoxic sediment pore waters. Conversely, the Os is likely to have been adsorbed from seawater by Mn(IV) oxyhydroxides following Mn(II) oxidation in the oxic portion of the water column and subsequently accumulated with the precipitation of authigenic Mn(II) carbonates following the reduction of Mn(IV) oxyhydroxides during organic matter oxidation in the sediment pile. More radiogenic Os_i values from the Mn carbonate ores, relative to those of the associated marlstones, are inferred to reflect an increased riverine influx that may have played a significant role in controlling the Mn mineralization of the Ortokarnash Mn deposit; however, more detailed paleogeographic data are required to fully evaluate that aspect of our model.

Acknowledgments

This work was supported by the National Science Foundation of China (No. U1703242 and 41902078), the Second Comprehensive Scientific Survey of the Qinghai- Tibet Plateau (2019QZKK0802), and the National Key R&D Program of China (No. 2018YFC0604001 and 2020YFA0714803). We are grateful to David Selby, Larry Meinert, and an anonymous reviewer for their insightful comments and suggestions. We also thank Zhuyin Chu and Yanhong Liu for their assistance in the laboratory. We are indebted to Changle Wang, Yang Li, and Xiqiang Zhou for constructive suggestions that significantly improved this manuscript. Hedong Li, Bin Zha, and Yueqiao Xie are thanked for their support during field work.

REFERENCES

Allègre, C.J., and Luck, J.M., 1980, Osmium isotopes as petrogenetic and geological tracers: Earth and Planetary Science Letters, v. 48, p. 148–154.

Anbar, A.D., Creaser, R.A., Papanastassiou, D.A., and Wasserburg, G.J., 1992, Rhenium in seawater: Confirmation of generally conservative behavior: Geochimica et Cosmochimica Acta, v. 56, p. 4099–4103.

Brumsack, H.J., 2006, The trace metal content of recent organic carbon-rich sediments: Implications for Cretaceous black shale formation: Palaeogeography, Palaeoclimatology, Palaeoecology, v. 232, p. 344–361.

Burton, K.W., Bourdon, B., Birck, J.L., Allègre, C.J., and Hein, J.R., 1999, Osmium isotope variations in the oceans recorded by Fe-Mn crusts: Earth and Planetary Science Letters, v. 171, p. 185–197.

Calvert, S.E., and Pedersen, T.F., 1996, Sedimentary geochemistry of manganese: Implications for the environment of formation of manganiferous black shales: Economic Geology, v. 91, p. 36–47.

Chen, J.T., Montaez, I.P., Qi, Y.P., Shen, S.Z., and Wang, X.D., 2018, Strontium and carbon isotopic evidence for decoupling of pCO_2 from continental weathering at the apex of the late Paleozoic glaciation: Geology, v. 46, p. 395–398.

Cleal, C.J., and Thomas, B.A., 2005, Palaeozoic tropical rainforests and their effect on global climates: is the past the key to the present?: Geobiology, v. 3, p. 13–31.

Colodner, D., Sachs, J.P., Ravizza, G.E., Turekian, K.K., Edmond, J.M., and Boyle, E.A., 1993, The geochemical cycle of rhenium: A reconnaissance: Earth and Planetary Science Letters, v. 117, p. 205–221.

Conrad, T.A., Nielsen, S.G., Peucker-Ehrenbrink, B., Blusztajn, J., Winslow, D., Hein, J.R., and Paytan, A., 2017, Reconstructing the evolution of the submarine Monterey Canyon system from Os, Nd, and Pb isotopes in hydrogenetic Fe-Mn crusts: Geochemistry, Geophysics, Geosystems, v. 18, p. 3946–3963.

Creaser, R.A., Sannigrahi, P., Chacko, T., and Selby, D., 2002, Further evaluation of the Re-Os geochronometer in organic-rich sedimentary rocks: A test of hydrocarbon maturation effects in the Exshaw Formation, western Canada sedimentary basin: Geochimica et Cosmochimica Acta, v. 66, p. 3441–3452.

Crusius, J., Calvert, S., Pedersen, T., and Sage, D., 1996, Rhenium and molybdenum enrichments in sediments as indicators of oxic, suboxic and sulfidic conditions of deposition: Earth and Planetary Science Letters, v. 145, p. 65–78.

Cumming, V. M., Selby, D., and Lillis, P. G., 2012, Re-Os geochronology of the lacustrine Green River Formation: Insights into direct depositional dating of lacustrine successions, Re-Os systematics and paleocontinental weathering: Earth and Planetary Science Letters, v. 359, p. 194–205.

Dellwig, O., Schnetger, B., Meyer, D., Pollehne, F., Hausler, K., and Arz, H.W., 2018, Impact of the major Baltic inflow in 2014 on manganese cycling in the Gotland Deep (Baltic Sea): Frontiers in Marine Science, v. 5, A. 248.

Dick, G.J., Clement, B.G., Webb, S.M., Fodrie, F.J., Bargar, J.R., and Tebo, B.M., 2009, Enzymatic microbial Mn(II) oxidation and Mn biooxide production in the Guaymas Basin deep-sea hydrothermal plume: Geochimica et Cosmochimica Acta, v.73, p. 6517–6530.

Dickson, A.J., Hsieh, Y.-T., and Bryan, A., 2020, The rhenium isotope composition of Atlantic Ocean seawater: Geochimica et Cosmochimica Acta, v. 287, p. 221–228.

Dubin, A., and Peucker-Ehrenbrink, B., 2015, The importance of organic-rich shales to the geochemical cycles of rhenium and osmium: Chemical Geology, v. 403, p. 111–120.

Esser, B.K., and Turekian, K.K., 1993, The osmium isotopic composition of the continental crust: Geochimica et Cosmochimica Acta, v. 57, p. 3093–3104.

Finlay, A.J., Selby, D., and Gröcke, D.R., 2010, Tracking the Hirnantian glaciation using Os isotopes: Earth and Planetary Science Letters, v. 293, p. 339–348.

Gao, Y., 2015, The confirming of Maerkanquekusaishan Formation in Kalaatehe belt in Western Kunlun Mountain, Xinjiang: Xinjiang Geology, v. 33, p. 290–294 (in Chinese with English abs.).

Gao, Y., Teng, J., Li , W., Chen, D., Sui, Q., Jing, D., He, Y., and Bai, J., 2018, Geology, geochemistry and ore genesis of the Aoertuokanashi manganese deposit, western Kunlun, Xinjiang, Northwest China: Acta Petrologica Sinica, v. 34, p. 2341–2358 (in Chinese with English abs.).

Goddéris, Y., Donnadieu, Y., Carretier, S., Aretz, M., Dera, G., Macouin, M., and Regard, V., 2017, Onset and ending of the late Palaeozoic ice age triggered by tectonically paced rock weathering: Nature Geoscience, v. 10, p. 382–386.

Gulbranson, E.L., Montanez, I.P., Schmitz, M.D., Limarino, C.O., Isbell, J.L., Marenssi, S.A., and Crowley, J.L., 2010, High-precision U-Pb calibration of Carboniferous glaciation and climate history, Paganzo Group, NW Argentina: Geological Society of America Bulletin, v. 122, p. 1480–1498.

Hannah, J.L., Bekker, A., Stein, H.J., Markey, R.J., and Holland, H.D., 2004, Primitive Os and 2316 Ma age for marine shale: Implications for Paleoproterozoic glacial events and the rise of atmospheric oxygen: Earth and Planetary Science Letters, v. 225, p. 43–52.

Hannah, J.L., Stein, H.J., Zimmerman, A., Yang, G., Markey, R.J., and Melezhik, V.A., 2006, Precise 2004 ± 9 Ma Re-Os age for Pechenga black shale: Comparison of sulfides and organic material: Geochimica et Cosmochimica Acta, v. 70, p. 228.

Hansel, C.M., Zeiner, C.A., Santelli, C.M., and Webb, S.M., 2012, Mn(II) oxidation by an ascomycete fungus is linked to superoxide production during asexual reproduction: Proceedings of the National Academy of Sciences of the United States of America, v. 109, p. 12,621–12,625.

Häusler, K., Dellwig, O., Schnetger, B., Feldens, P., Leipe, T., Moros, M., Pollehne, F., Schönke, M., Wegwerth, A., and Arz, H.W., 2018, Massive Mn carbonate formation in the Landsort Deep (Baltic Sea): Hydrographic conditions, temporal succession, and Mn budget calculations: Marine Geology, v. 395, p. 260–270.

Huckriede, H., and Meischner, D., 1996, Origin and environment of manganese-rich sediments within black-shale basins: Geochimica et Cosmochimica Acta, v. 60, p. 1399–1413.

Jin, X.D., Li, W.J., Xiang, P., Sakyi, P.A., Zhu, M.T., and Zhang, L.C., 2013, A contribution to common Carius tube distillation techniques: Journal of Analytical Atomic Spectrometry, v. 28, p. 396–404.

Johnson, J.E., Webb, S.M., Ma, C., and Fischer, W.W., 2016, Manganese mineralogy and diagenesis in the sedimentary rock record: Geochimica et Cosmochimica Acta, v. 173, p. 210–231.

Josso, P., Parkinson, I., Horstwood, M., Lusty, P., Chenery, S., and Murton, B., 2019, Improving confidence in ferromanganese crust age models: A composite geochemical approach: Chemical Geology, v. 513, p. 108–119.

Kendall, B., van Acken, D., and Creaser, R.A., 2013, Depositional age of the early Paleoproterozoic Klipputs Member, Nelani Formation (Ghaap Group, Transvaal Supergroup, South Africa) and implications for low-level Re-Os geochronology and Paleoproterozoic global correlations: Precambrian Research, v. 237, p. 1–12.

Klemm, V., Levasseur, S., Frank, M., Hein, J.R., and Halliday, A.N., 2005, Osmium isotope stratigraphy of a marine ferromanganese crust: Earth and Planetary Science Letters, v. 238, p. 42–48.

Kristin D.B., John P.G., and Woodward W.F., 2013, Biological influences on seafloor carbonate precipitation: Palaios, v. 28, p. 99–115.

Konhauser, K.O., 2007, Introduction to geomicrobiology: Blackwell, Oxford, p.425.

Li, Y., Zhang, S., Hobbs, R., Caiado, C., Sproson, A.D., Selby, D., and Rooney, A.D., 2019, Monte Carlo sampling for error propagation in linear regression and applications in isochron geochronology: Science Bulletin, v. 64, p. 51–59.

Liu, T., Maynard, J.B., and Alten, J., 2006, Superheavy S isotopes from glacier-associated sediments of the Neoproterozoic of south China: Oceanic anoxia or sulfate limitation?: Geological Society of America Memoirs, v. 198, p. 205–222.

Lu, X., Kendall, B., Stein, H.J., and Hannah, J.L., 2017, Temporal record of osmium concentrations and $^{187}Os/^{188}Os$ in organic-rich mudrocks: Implications for the osmium geochemical cycle and the use of osmium as a paleoceanographic tracer: Geochimica et Cosmochimica Acta, v. 216, p. 221–241.

Ludwig, K., 2012, Isoplot/Ex Version 3.75, A geochronological toolkit for Microsoft Excel: Berkeley Geochronology Center, Berkeley, California, Special Publication 5, 75p.

Maliva, R.G., Dickson, J.D., and Fallick, A.E., 1999, Kaolin cements in limestones; potential indicators of organic-rich pore waters during diagenesis: Journal of Sedimentary Research, v. 69, p. 158–163.

Marin, B., and Giresse, P., 2001, Particulate manganese and iron in recent sediments of the Gulf of Lions continental margin (north-western Mediterranean Sea): Deposition and diagenetic process: Marine Geology, v. 172, p. 147–165.

Maynard, J.B., 2010, The chemistry of manganese ores through time: a signal of increasing diversity of earth-surface environments: Economic Geology, v. 105, p. 535–552.

—— 2014, Manganiferous sediments, rocks, and ores: Treatise on Geochemistry, v. 9, p. 327–349.

McDaniel, D.K., Walker, R.J., Hemming, S.R., Horan, M.F., Becker, H., and Grauch, R.I., 2004, Sources of osmium to the modern oceans: New evidence from the ^{190}Pt-^{186}Os system: Geochimica et Cosmochimica Acta, v. 68, p. 1243–1252.

Meister, P., Bernasconi, S.M., Aiello, I.W., Vasconcelos, C., and Mckenzie, J.A., 2009, Depth and controls of Ca-rhodochrosite precipitation in bioturbated sediments of the Eastern Equatorial Pacific, ODP Leg 201, Site 1226 and DSDP Leg 68, Site 503: Sedimentology, v. 56, p. 1552–1568.

Miller, C.A., Peucker-Ehrenbrink, B., Walker, B.D., and Marcantonio, F., 2011, Re-assessing the surface cycling of molybdenum and rhenium: Geochimica et Cosmochimica Acta, v. 75, p. 7146–7179.

Morford, J.L., Emerson, S.R., Breckel, E.J., and Kim, S.H., 2005, Diagenesis of oxyanions (V, U, Re, and Mo) in pore waters and sediments from a continental margin: Geochimica et Cosmochimica Acta, v. 69, p. 5021–5032.

Morgan, J.W., Horan, M.F., Walker, R.J., and Grossman, J.N., 1995, Rhenium-osmium concentration and isotope systematics in group IIab iron-meteorites: Geochimica et Cosmochimica Acta, v. 59, p. 2331–2344.

Neumann, T., Heiser, U., Leosson, M.A., and Kersten, M., 2002, Early diagenetic processes during Mn-carbonate formation: evidence from the isotopic composition of authigenic Ca-rhodochrosites of the Baltic Sea: Geochimica et Cosmochimica Acta, v. 66, p. 867–879.

Oxburgh, R., 1998, Variations in the osmium isotope composition of sea water over the past 200,000 years: Earth and Planetary Science Letters, v. 159, p. 183–191.

Pan, Y.S., and Fang, A.M., 2010, Formation and evolution of the Tethys in the Tibetan plateau: Chinese Journal of Geology, v. 45, p. 92–101 (in Chinese with English abs.).

Paquay, F.S., Ravizza, G., and Coccioni, R., 2014, The influence of extraterrestrial material on the late Eocene marine Os isotope record: Geochimica et Cosmochimica Acta, v. 144, p. 238–257.

Peucker-Ehrenbrink, B., and Jahn, B.M., 2001, Rhenium-osmium isotope systematics and platinum group element concentrations: Loess and the upper continental crust: Geochemistry, Geophysics, Geosystems, v. 2, p. 2001GC000172.

Peucker-Ehrenbrink, B., and Ravizza, G.E., 2000, The marine osmium isotope record: Terra Nova, v. 12, p. 205–219.

—— 2020, Osmium isotope stratigraphy, *in* Gradstein, F.M., Ogg, J.G., Ogg, G.M., and Schmitz, M.D., ed., Geologic Time Scale, Elsevier, p. 239–257.

Pietras, J.T., Selby, D., Brembs, R., Dennett, A., 2020, Tracking drainage basin evolution, continental tectonics, and climate change: Implications from osmium isotopes of lacustrine systems: Palaeogeography, Palaeoclimatology, Palaeoecology, v. 537, p. 109471.

Ravizza, G., and Peucker-Ehrenbrink, B., 2003, The marine $^{187}Os/^{188}Os$ record of the Eocene-Oligocene transition: The interplay of weathering and glaciation: Earth and Planetary Science Letters, v. 210, p. 151–165.

Ravizza G., and Turekian K.K., 1989, Application of the 187Re-187Os system to black shale geochronometry: Geochimica Et Cosmochimica Acta, v. 53, p. 3257–3262.

—— 1992, The osmium isotopic composition of organic-rich marine sediments: Earth and Planetary Science Letters, v. 110 p. 1–6.

Ravizza, G., Turekian, K.K., and Hay, B.J., 1991, The geochemistry of rhenium and osmium in recent sediments from the Black Sea: Geochimica et Cosmochimica Acta, v. 55, p. 3741–3752.

Rooney, A.D., Selby, D., Houzay, J.P., and Renne, P.R., 2010, Re-Os geochronology of a Mesoproterozoic sedimentary succession, Taoudeni basin, Mauritania: Implications for basin-wide correlations and Re-Os organic-rich sediments systematics: Earth and Planetary Science Letters, v. 289, p. 486–496.

Rooney, A.D., Chew, D.M., and Selby, D., 2011, Re-Os geochronology of the Neoproterozoic-Cambrian Dalradian Supergroup of Scotland and Ireland: Implications for Neoproterozoic stratigraphy, glaciations and Re-Os systematics: Precambrian Research, v. 185, p. 202–214.

Rooney, A.D., Selby, D., Lewan, M., Lillis, P.G., and Houzay, J.P., 2012, Evaluating Re–Os systematics in organic-rich sedimentary rocks in response to petroleum generation using hydrous pyrolysis experiments: Geochimica et Cosmochimica Acta, v. 77, p. 275–291.

Rooney, A.D., Yang, C., Condon, D.J., Zhu, M., and Macdonald, F.A., 2020, U-Pb and Re-Os geochronology tracks stratigraphic condensation in the Sturtian snowball Earth aftermath: Geology, v. 48, p. 625–629.

Rotich, E.K., Handler, M.R., Sykes, R., Selby, D., and Naeher, S., 2021, Depositional influences on Re-Os systematics of Late Cretaceous-Eocene fluvio-deltaic coals and coaly mudstones, Taranaki basin, New Zealand: International Journal of Coal Geology, v. 236, p. 103670.

Selby, D., and Creaser, R.A., 2003, Re-Os geochronology of organic rich sediments: An evaluation of organic matter analysis methods: Chemical Geology, v. 200, p. 225–240.

Selby, D., Mutterlose, J., and Condon, D.J., 2009, U-Pb and Re-Os geochronology of the Aptian/Albian and Cenomanian/Turonian stage boundaries: Implications for timescale calibration, osmium seawater composition and Re-Os systematics in organic-rich sediments: Chemical Geology, v. 265, p. 394–409.

Sharma, M., Wasserburg, G.J., Hofmann, A.W., and Butterfield, D.A., 2000, Osmium isotopes in hydrothermal fluids from the Juan de Fuca Ridge: Earth and Planetary Science Letters, v. 179, p. 139–152.

Sheen, A.I., Kendall, B., Reinhard, C.T., Creaser, R.A., Lyons, T.W., Bekker, A., Poulton, S.W., and Anbar, A.D., 2018, A model for the oceanic mass balance of rhenium and implications for the extent of Proterozoic ocean anoxia: Geochimica et Cosmochimica Acta, v. 227, p. 75–95.

Smoliar, M.I., Walker, R.J., and Morgan, J.W., 1996, Re-Os ages of group IIA, IIIA, IVA, and IVB iron meteorites: Science, v. 271, p. 1099–1102.

Tebo, B.M., Bargar, J.R., Clement, B.G., Dick, G.J., Murray, K.J., Parker, D., Verity, R., and Webb, S.M., 2004, Biogenic manganese oxides: Properties and mechanisms of Formation: Annual Review of Earth and Planetary Sciences, v. 32, p. 287–328.

Thamdrup, B., Rosselló-Mora, R., and Amann, R., 2000, Microbial manganese and sulfate reduction in Black Sea Shelf sediments: Applied and Environmental Microbiology, v. 66, p. 2888–2897.

Tokumaru, A., Nozaki, T., Suzuki, K., Goto, K.T., Chang, Q., Kimura, J.I., Takaya, Y., Kato, Y., Usui, A., and Urabe, T., 2015, Re-Os isotope geochemistry in the surface layers of ferromanganese crusts from the Takuyo Daigo Seamount, northwestern Pacific Ocean: Geochemical Journal, v. 49, p. 233–241.

Tripathy, G.R., Hannah, J.L., Stein, H.J., and Yang, G., 2014, Re-Os age and depositional environment for black shales from the Cambrian-Ordovician boundary, Green Point, western Newfoundland: Geochemistry, Geophysics, Geosystems, v. 15, p. 1021–1037.

Tripathy, G.R., Hannah, J.L., Stein, H.J., Geboy, N.J., and Ruppert, L.F., 2015, Radiometric dating of marine-influenced coal using Re-Os geochronology: Earth and Planetary Science Letters, v. 432, p. 13–23.

Xu, G., Hannah, J.L., Stein, H.J., Mørk, A., Vigran, J., Bingen, B., Schutt, D., and Lund-schien, B., 2014, Cause of Upper Triassic climate crisis revealed by Re–Os geochemistry of Boreal black shales: Palaeogeography, Palaeoclimatology, Palaeoecology, v. 395, p. 222–232.

Yamashita, Y., Takahashi, Y., Haba, H., Enomoto S.,and Shimizu H., 2007, Comparison of reductive accumulation of Re and Os in seawater-sediment systems: Geochimica et Cosmochimica Acta, v. 71, p. 3458–3475.

Yin, A., and Harrison, T.M., 2000., Geologic evolution of the Himalayan-Tibetan orogen: Annual Review of Earth and Planetary Sciences, v. 28, p. 211–280.

Yu, W., Algeo, T.J., Du, Y., Maynard, B., Guo, H., Zhou, Q., Peng, T., Wang, P., and Yuan, L., 2016, Genesis of Cryogenian Datangpo manganese deposit: Hydrothermal influence and episodic post-glacial ventilation of Nanhua basin, South China: Palaeogeography, Palaeoclimatology, Palaeoecology, v. 459, p. 321–337.

Zhang, B.L., 2020, Depositional environment and mineralization mechanism of the gaint Ortokarnash manganese carbonate deposit in the Western Kunlun Mountains: Ph.D. thesis, Institute of Geology and Geophysics, Chinese Academy of Sciences, 222 p.

Zhang, B.L., Zhang, L.C., Feng, J., Xu, S.Q., Feng, C.R., Hao, Y.H., Zheng, M.T., Peng, Z.D., and Dong, Z.G., 2018, Genesis of the large-scale Orto Karnash manganese carbonate deposit in the Malkansu district, Western Kunlun: Evidence from geological features: Geological Review, v. 64, p. 361–377 (in Chinese with English abs.).

Zhang, B.L., Wang, C.L., Robbins, J., Zhang, L.C., Konhauser, K.O., Dong, Z.G., Li, W.J., Peng, Z.D., and Zheng, M.T., 2020, Petrography and geochemistry of the Carboniferous Ortokarnash manganese deposit in the Western Kunlun Mountains, Xinjiang Province, China: Implications for the Depositional Environment and the Origin of Mineralization: Economic Geology, v. 115, p. 1559–1588.

Zhao, H., Li, C., Jiang, X.J., Zhou, L.M., Li, X.W., Qu, W.J., and Du, A.D., 2015, Enrichment mechanism of Re-Os in limestone from Changxing Permian-Triassic boundary in Zhejiang: Acta Geologica Sinica, v. 89, p. 1783–1791 (in Chinese with English abs.).

Wenjun Li is a senior engineer at the Mineralization Elements and Isotopes Laboratory at the Institute of Geology and Geophysics, Chinese Academy of Sciences (IGGCAS). She is also a Ph.D. candidate in economic geology at IGGCAS. She received her B.S. degree in applied chemistry from China University of Geosciences, Beijing (CUGB), China. Her research focuses on the genesis of sedimentary manganese and analysis of Re-Os geochronology, trace elements by LA-ICP-MS, as well as potassium isotopes in the near future.